the plant journal

SEB Society for Experimental Biology

The Plant Journal (2018) **94,** 1023–1037 doi: 10.1111/tpj.13915

GreenCut protein CPLD49 of *Chlamydomonas reinhardtii* associates with thylakoid membranes and is required for cytochrome b_6f complex accumulation

Tyler M. Wittkopp[1,2,†], Shai Saroussi[2,†], Wenqiang Yang[2], Xenie Johnson[3], Rick G. Kim[1,2], Mark L. Heinnickel[2], James J. Russell[1], Witchukorn Phuthong[4], Rachel M. Dent[5,6], Corey D. Broeckling[7], Graham Peers[8], Martin Lohr[9], Francis-André Wollman[10], Krishna K. Niyogi[5,6] and Arthur R. Grossman[2,*]

[1]*Department of Biology, Stanford University, Stanford, CA 94305, USA,*

[2]*Department of Plant Biology, Carnegie Institution for Science, Stanford, CA 94305, USA,*

[3]*Laboratoire de Bioénergétique et Biotechnologie des Bactéries et Microalgues, CEA Cadarache, Saint Paul lez Durance, France,*

[4]*Department of Materials Science and Engineering, Stanford University, Stanford, CA 94305, USA,*

[5]*Department of Plant and Microbial Biology, Howard Hughes Medical Institute, University of California, Berkeley, CA 94720-3102, USA,*

[6]*Molecular Biophysics and Integrated Bioimaging Division, Lawrence Berkeley National Laboratory, Berkeley, CA 94720, USA,*

[7]*Proteomics and Metabolomics Facility, Colorado State University, Fort Collins, CO 80523, USA,*

[8]*Department of Biology, Colorado State University, Fort Collins, CO 80523, USA,*

[9]*Institut für Molekulare Physiologie – Pflanzenbiochemie, Johannes Gutenberg-Universität, 55099 Mainz, Germany, and*

[10]*Institut de Biologie Physico-Chimique, CNRS-UPMC, Paris, France*

Received 27 October 2017; revised 23 February 2018; accepted 6 March 2018; published online 30 March 2018.

*For correspondence (e-mail agrossman@carnegiescience.edu).

†These authors contributed equally to this work.

SUMMARY

The GreenCut encompasses a suite of nucleus-encoded proteins with orthologs among green lineage organisms (plants, green algae), but that are absent or poorly conserved in non-photosynthetic/heterotrophic organisms. In *Chlamydomonas reinhardtii*, CPLD49 (Conserved in Plant Lineage and Diatoms49) is an uncharacterized GreenCut protein that is critical for maintaining normal photosynthetic function. We demonstrate that a *cpld49* mutant has impaired photoautotrophic growth under high-light conditions. The mutant exhibits a nearly 90% reduction in the level of the cytochrome b_6f complex (Cytb_6f), which impacts linear and cyclic electron transport, but does not compromise the ability of the strain to perform state transitions. Furthermore, CPLD49 strongly associates with thylakoid membranes where it may be part of a membrane protein complex with another GreenCut protein, CPLD38; a mutant null for CPLD38 also impacts Cytb_6f complex accumulation. We investigated several potential functions of CPLD49, with some suggested by protein homology. Our findings are congruent with the hypothesis that CPLD38 and CPLD49 are part of a novel thylakoid membrane complex that primarily modulates accumulation, but also impacts the activity of the Cytb_6f complex. Based on motifs of CPLD49 and the activities of other CPLD49-like proteins, we suggest a role for this putative dehydrogenase in the synthesis of a lipophilic thylakoid membrane molecule or cofactor that influences the assembly and activity of Cytb_6f.

Keywords: GreenCut, photosynthesis, cytochrome b_6f, electron transport, chloroplast, thylakoid membranes, CPLD38, dehydrogenase.

INTRODUCTION

Oxygenic photosynthesis involves the capture of solar energy by thylakoid membrane pigment–protein complexes and coupled electron transfer reactions that convert absorbed light to chemical bond energy. Solar energy is absorbed by light-harvesting complexes I (LHCI) and II (LHCII) that are associated with photosystems I and II (PSI

and PSII, respectively) reaction centers. Excited PSII reaction centers generate the oxidative environment that enables the splitting of water, which liberates O_2, H^+ and electrons. The electrons are transferred from PSII to PSI via the plastoquinone (PQ) pool, the cytochrome b_6f complex (Cytb_6f) and the mobile electron carrier plastocyanin (PC), to ultimately reduce ferredoxin and $NADP^+$, which function as electron donors in anabolic metabolism. This electron transport pathway is known as linear electron flow (LEF). In contrast, cyclic electron flow (CEF) involves the transfer of electrons in a cycle around PSI. Although CEF does not generate NADPH, like LEF it is coupled to the establishment of a transmembrane H^+ gradient that drives ATP formation by the chloroplast ATP synthase; both LEF and CEF require Cytb_6f.

Assembly of the photosynthetic machinery involves coordinated synthesis of nucleus- and chloroplast-encoded polypeptides along with the pigment molecules with which they associate (Eberhard *et al.*, 2008; Lyska *et al.*, 2013). Recently, several factors necessary for assembly of PSII, PSI and Cytb_6f were identified in cyanobacteria, algae and plants (Rochaix, 2004, 2011; Schöttler *et al.*, 2011; Chi *et al.*, 2012; Heinnickel *et al.*, 2013, 2016; Nickelsen and Rengstl, 2013; Hartings *et al.*, 2017; Wittenberg *et al.*, 2017). For the unicellular green alga *Chlamydomonas reinhardtii* (Chlamydomonas throughout), Cytb_6f assembly requires a class of proteins that facilitates integration of heme into apocytochrome b_6 and apocytochrome *f* (Inoue *et al.*, 1997; Xie *et al.*, 1998; Kuras *et al.*, 2007; Gabilly *et al.*, 2010; Cline *et al.*, 2017). Many Chlamydomonas mutants have been identified that are defective for the synthesis of Cytb_6f, which involves both translational and post-translational control (Kuras and Wollman, 1994; Choquet *et al.*, 1998). Interestingly, regulation of translation of mRNAs for the chloroplast-encoded Cytb_6f subunits operates through a process designated CES ('controlled by epistatic synthesis'; Wollman *et al.*, 1999; Choquet and Vallon, 2000; Choquet and Wollman, 2002; Choquet *et al.*, 2003), in which a free subunit of the complex depresses translation initiation of the mRNA encoding that subunit. A similar mechanism controls the biogenesis of PSI (Wostrikoff *et al.*, 2004).

We previously identified a thylakoid membrane protein designated CPLD38, which is necessary for proper accumulation of Cytb_6f (Heinnickel *et al.*, 2013). The Chlamydomonas *cpld38* mutant accumulates approximately 25% of wild-type (WT) levels of Cytb_6f, potentially the consequence of accelerated degradation of this complex. This mutant is also sensitive to high light (HL), and has a growth defect under photoautotrophic conditions (Heinnickel *et al.*, 2013). An *Arabidopsis thaliana* (Arabidopsis hereafter) mutant lacking the CPLD38 ortholog, designated DAC (Defective Accumulation of Cytochrome b_6f complex), displayed a similar phenotype (Xiao *et al.*, 2012). While DAC may interact with the PetD subunit of the Cytb_6f complex, the mechanism by which it impacts the levels of the complex is not understood (Xiao *et al.*, 2012).

To identify additional proteins involved in synthesis, assembly and stability of photosynthetic complexes, we examined Chlamydomonas mutants disrupted in genes encoding various GreenCut proteins. The GreenCut is a bioinformatically derived protein inventory present in green lineage (photosynthetic) organisms, but absent or poorly conserved in heterotrophic (non-photosynthetic) organisms (Merchant *et al.*, 2007; Karpowicz *et al.*, 2011; Heinnickel and Grossman, 2013; Wittkopp *et al.*, 2016). Many GreenCut proteins function within chloroplasts, where they are involved in diverse processes ranging from assembly of photosynthetic complexes to influencing electron transport and carbon fixation (Schult *et al.*, 2007; Dobáková *et al.*, 2009; Armbruster *et al.*, 2010; Karamoko *et al.*, 2011; Kirst *et al.*, 2012; Link *et al.*, 2012; Mininno *et al.*, 2012; Xiao *et al.*, 2012; Calderon *et al.*, 2013; Heinnickel *et al.*, 2013, 2016; Fristedt *et al.*, 2014, 2015; Bhuiyan *et al.*, 2015; Wittkopp *et al.*, 2016). Mutants defective for genes encoding GreenCut proteins have been isolated using both forward (Dent *et al.*, 2005, 2015) and reverse (Pootakham *et al.*, 2010; Gonzalez-Ballester *et al.*, 2011) genetic screens. In this work, we analyze a Chlamydomonas strain that is unable to synthesize the GreenCut protein CPLD49, and demonstrate that this protein plays a critical role in: (i) maintaining normal photosynthetic electron transport; (ii) the accumulation of the Cytb_6f complex; and (iii) survival during exposure of cells to HL under photoautotrophic conditions. Furthermore, CPLD49 associates with thylakoid membranes where it may interact with CPLD38, a GreenCut protein also critical for Cytb_6f complex accumulation.

RESULTS

CPLD49 is necessary for photoautotrophic growth in HL

The Chlamydomonas Cre16.g666050 locus encodes CPLD49, a GreenCut protein of 448 amino acids with a predicted N-terminal chloroplast transit peptide (Tardiff *et al.*, 2012), two saccharopine dehydrogenase domains (Marchler-Bauer *et al.*, 2015) and no predicted transmembrane sequences (Figure 1a). A partial characterization of the CAL014.01.15 mutant first suggested a critical role for CPLD49 (Cre16.g666050) in photosynthesis (Dent *et al.*, 2015). This mutant, which has an insertional disruption in Cre16.g666050, was described as acetate-requiring, suggesting impairment in photoautotrophic growth (Dent *et al.*, 2015). Based on sequence analysis of CAL014.01.15, we determined that the pMS188 cassette (used for random mutagenesis) was inserted into chromosome 16, creating a 26 918 bp deletion at the insertion site that completely deleted four genes and disrupted two others (Figures 1b

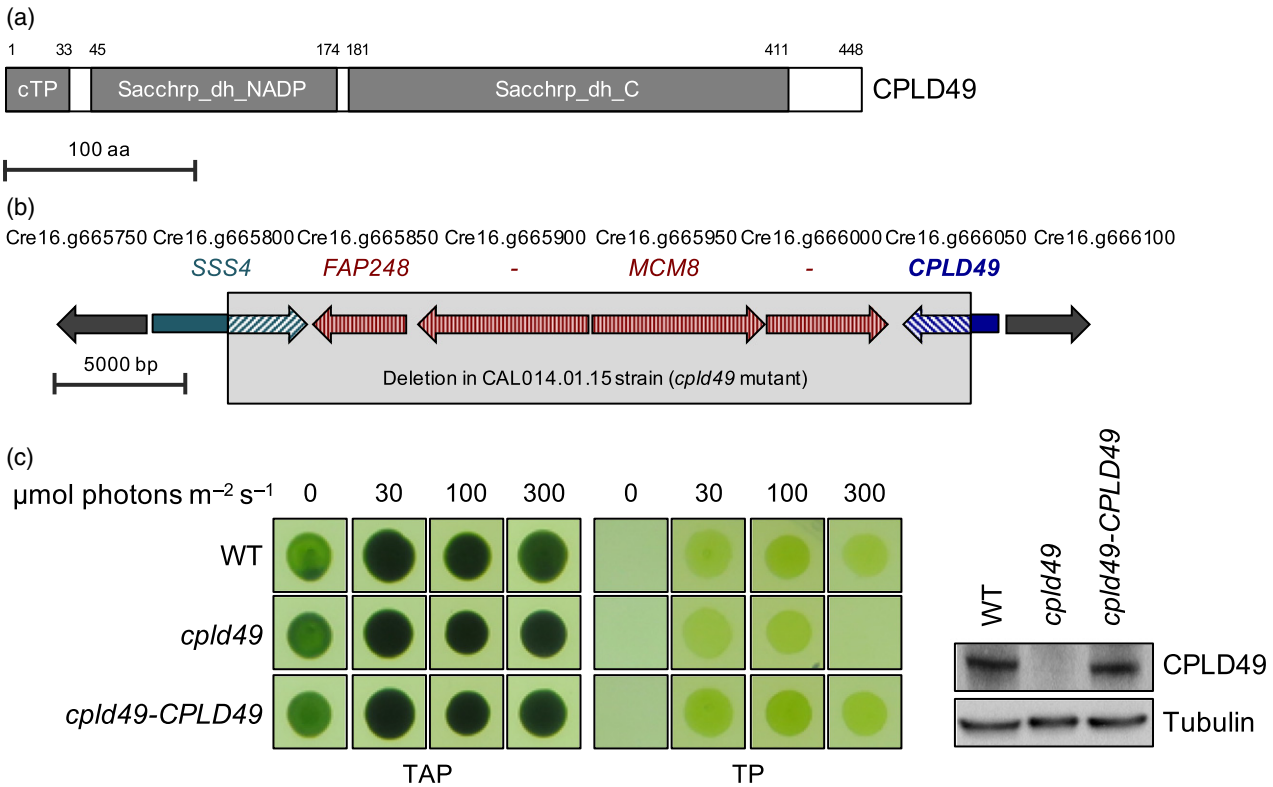

Figure 1. Loss of CPLD49 in CAL014.01.15 causes compromised photoautotrophic growth in high light (HL).
(a) Protein domains of CPLD49 showing the chloroplast transit peptide (cTP) and saccharopine dehydrogenase NADP binding and C-terminal saccharopine dehydrogenase domains. The number of the first and last amino acid of each domain is indicated.
(b) Site of insertion of the *pMS188* cassette into the Chlamydomonas genome in the *cpld49* mutant (CAL014.01.15; the insertion displaced the shaded boxed region). Four gene models on chromosome 16 were completely deleted, and two others, including *CPLD49* (Cre16.g666050), were truncated. The sites at which the vector caused truncation of Cre16.g665800 and Cre16.g666050 genes are shown. Additional details of the insertion are given in Figure S1(a).
(c) Growth of the *cpld49* mutant under photoheterotrophic conditions [Tris–Acetate–Phosphate (TAP) agar, left] and photoautotrophic conditions [Tris–Phosphate (TP) agar, right] at different light intensities. Medium containing 10^5 cells was spotted onto agar plates and grown for 7 days. Growth light intensities are indicated.
(d) Immunoblot of CPLD49 accumulation in wild-type (WT), *cpld49* and *cpld49-CPLD49*. Tubulin was used as a loading control.

and S1). Among the genes deleted or disrupted by the insertion event in CAL014.01.15 is *CPLD49* (Cre16.g666050), which is the only gene of the disrupted cluster that encodes a protein confirmed by proteomic analysis to be chloroplast-localized (Table S1; Terashima *et al.*, 2011). DNA blot hybridizations revealed that a single pMS188 cassette had incorporated into the genome of the mutant (Figure S2). Importantly, the photosynthetic phenotype of the mutant was also observed in two independent *cpld49* mutant alleles (see below) and fully rescued by ectopic expression of *CPLD49*; therefore, the CAL014.01.15 strain is hereafter referred to as the *cpld49* mutant.

To evaluate growth and light sensitivity of *cpld49*, it was backcrossed three times to WT (see Experimental Procedures) and spotted onto Tris–Acetate–Phosphate (TAP) and Tris–Phosphate (TP) agar medium. When *cpld49* was grown heterotrophically or photoheterophically on TAP medium (in darkness or light, respectively, with acetate as an external carbon source) for 7 days, the mutant did not exhibit a growth defect regardless of the light intensity to which the cells were exposed [i.e. 30, 100 and 300 μmol photons m^{-2} sec^{-1}; hereafter low light (LL), moderate light (ML) and HL, respectively; Figure 1c, left]. To test whether *cpld49* requires an external carbon source for normal growth, we simultaneously performed the spotting assay using photoautotrophic (TP) medium. Growth of *cpld49* on TP under LL or ML was similar to that of WT, while it was unable to grow photoautotrophically when exposed to HL (Figure 1c, right). Introduction of a WT genomic copy of *CPLD49* into the *cpld49* mutant restored photoautotrophic growth in HL on solid medium (Figure 1c; complemented strain designated *cpld49-CPLD49*), suggesting that disruption of *CPLD49* in CAL014.01.15 is responsible for the observed growth defect on TP medium. Additionally, an antibody was raised to CPLD49 and immunoblots were performed using total protein extracts from WT, *cpld49* and the *cpld49-CPLD49* rescued strain. The results confirmed that

cpld49 does not accumulate CPLD49 protein (apparent MW ~49 kDa), while *cpld49-CPLD49* showed restoration of CPLD49 accumulation to a level comparable to that of WT cells (Figure 1d).

Growth of the *cpld49* mutant was also impaired in liquid medium. In the presence of acetate, the *cpld49* mutant grew at a similar rate to that of WT and *cpld49-CPLD49* in LL, achieving a slightly higher cell density in HL (Figure S3a, left panels). On a per Chl basis, all strains exhibited similar growth rates in TAP (Figure S3b, left panels). In the absence of acetate, growth of *cpld49* was indistinguishable from WT and *cpld49-CPLD49* in LL with respect to both cell density and Chl concentration (Figure S3a,b, right panels). However, as observed on solid medium, *cpld49* failed to grow photoautotrophically in HL (Figure S3a,b, right panels, and c). These results suggest that a defect in photosynthesis limits growth of *cpld49*, especially under conditions of high photon flux. An external carbon source (i.e. acetate) may energetically compensate for low photosynthetic yields associated with elevated light levels, enabling HL growth on TAP but not TP.

Loss of CPLD49 impacts photosynthetic electron transport

The inability of the *cpld49* mutant to grow photoautotrophically in HL suggests that the strain is photosynthetically defective. To evaluate photosynthetic activity, all strains were grown photoheterotrophically under LL and HL, and photoautotrophically in LL, and photosynthetic electron transport was assayed using Chl fluorescence induction kinetics (Figures 2a,b and S4a). When grown photoheterotrophically in LL, the *cpld49* mutant had a slightly higher level of steady-state fluorescence (F′) than WT and *cpld49-CPLD49* (Figure 2a), suggesting a constriction in electron transport downstream of PSII (Baker, 2008). The F′ level was even higher for HL, photoheterotrophically grown *cpld49* (relative to WT), suggesting a more pronounced defect in electron flow (Figure 2b). Additional photosynthetic parameters derived from Chl fluorescence

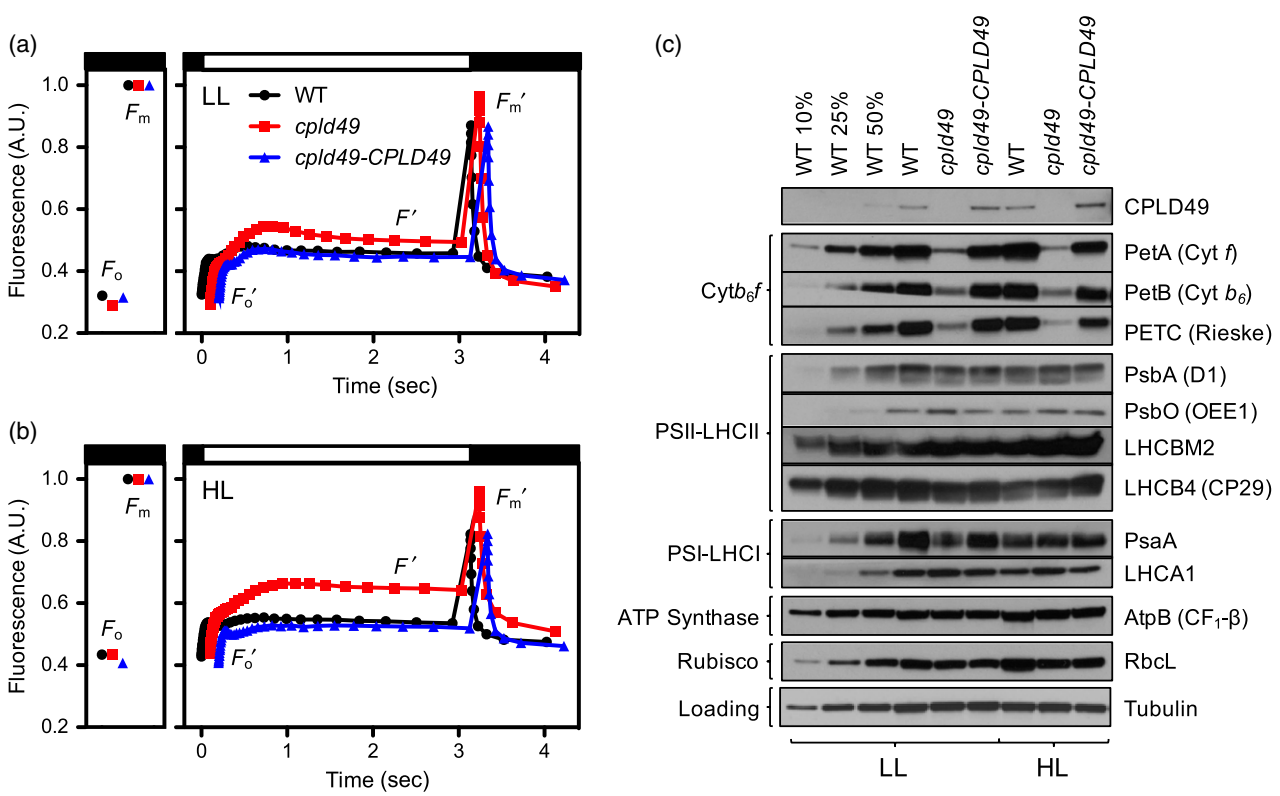

Figure 2. The *cpld49* mutant is impaired in photosynthetic electron transport and deficient in Cytb_6f accumulation.
(a, b) Chl fluorescence measurements showing F_o, F_m values (left panels) and Chl fluorescence induction kinetics (right panels) for wild-type (WT), *cpld49* and *cpld49-CPLD49* cultures grown photoheterotrophically in low light (LL) and high light (HL). The LL (a) and HL (b) grown strains were dark-adapted prior to measuring F_o, F_m and fluorescence induction kinetics at 156 μmol photons m^{-2} sec^{-1} actinic light. A saturating light pulse was administered to determine F_m and F_m'. Data were normalized to F_m values for each strain. Dark (filled) and light (unfilled) periods are indicated above each set of curves. Curves are slightly offset on *x*-axis. F_o, minimum fluorescence in the dark; F_o', minimum fluorescence in the light; F′, steady-state fluorescence in the light; F_m, maximum fluorescence in the dark; F_m', maximum fluorescence in the light.
(c) Immunoblot analysis of representative photosynthetic pigment–protein complex subunits from cells grown photoheterotrophically in LL and HL. A dilution series is provided for WT grown in LL (10–100%). Tubulin was used as a loading control.

Table 1 Measurement of photosynthetic parameters after photoheterotrophic growth

Growth light	Parameter	WT	*cpld49*	*cpld49-CPLD49*
LL	F_v/F_m	0.689 ± 0.013	0.683 ± 0.040	0.666 ± 0.027
	ΦPSII (AL: 156)	0.479 ± 0.007	0.405 ± 0.046	0.473 ± 0.004
	ΦPSII (AL: 530)	0.322 ± 0.006	0.177 ± 0.043	0.328 ± 0.024
HL	F_v/F_m	0.539 ± 0.038	0.571 ± 0.007	0.576 ± 0.024
	ΦPSII (AL: 156)	0.472 ± 0.026	0.354 ± 0.028	0.464 ± 0.015
	ΦPSII (AL: 530)	0.352 ± 0.003	0.129 ± 0.013	0.348 ± 0.006

Strains were grown in TAP medium in either LL (30 μmol photons m^{-2} sec^{-1}) or HL (300 μmol photons m^{-2} sec^{-1}). Assays were performed using actinic light (AL) of either 156 or 530 μmol photons m^{-2} sec^{-1}. F_v/F_m and ΦPSII values were obtained from Chl fluorescence measurements. Average ± SD values are reported for three biological replicates.
HL, high light; LL, low light; WT, wild-type.

measurements under photoheterotrophic conditions are provided in Table 1. The maximum quantum yield of PSII (F_v/F_m) is similar for all strains grown in LL and HL (Table 1), suggesting that reduced electron flow in *cpld49* is not the consequence of altered PSII activity, but rather a block downstream of PSII. In accord with this finding, the quantum yield of PSII (ΦPSII) in photoheterotrophically grown *cpld49* decreases with increasing growth light intensity (Table 1). Importantly, these mutant phenotypes were rescued in the *cpld49-CPLD49* complemented strain (Figures 2, 3 and S4a; Table 1).

cpld49 has reduced Cytb_6f accumulation

To determine whether the photosynthetic characteristics observed in *cpld49* were a consequence of altered accumulation of specific proteins or pigment–protein complexes associated with photosynthetic function, we isolated total protein from cells grown photoheterotrophically in LL and HL, and photoautotrophically in LL (Figures 2c and S4b). Proteins were resolved by sodium dodecyl sulfate–polyacrylamide gel electrophoresis (SDS–PAGE), and immunoblots performed using antibodies specific for the protein subunits of the major photosynthetic complexes. Subunits of PSII (PsbA or D1), the oxygen evolving complex (PsbO or OEE1), LHCII (LHCBM2; LHCB4 or CP29), LHCI (LHCA1), the chloroplast ATP synthase (AtpB or CF_1-β) and Rubisco (RbcL, large subunit) accumulated to near WT levels in *cpld49* under both LL and HL conditions (Figure 2c). Some reduction of PSI (PsaA) was observed in *cpld49*, but only in LL (Figure 2c). In contrast, *cpld49* exhibited strongly diminished levels of Cytb_6f subunits (~10% of WT levels) during growth in both LL and HL, as represented by PetA (Cyt *f*), PetB (Cyt b_6) and PETC (Rieske iron-sulfur protein; Figure 2c). We also determined if the loss of CPLD49 had a broader impact on the architecture of the photosynthetic apparatus by quantifying the PSI:PSII ratio using the single laser-flash electrochromic shift assay. For cells grown photoheterotrophically in HL, the PSI:PSII ratio for all three strains was similar (1.73 ± 0.17, 1.64 ± 0.21 and 1.5 ± 0.26 for WT, *cpld49* and *cpld49-CPLD49*, respectively; *t*-test *P*-value >0.05; $n = 6$ for each strain), implying no significant alteration in photosystem stoichiometry. Hence, the loss of CPLD49 specifically affects Cytb_6f accumulation with little impact on other major photosynthetic complexes. The reduced rate of electron transport because of decreased Cytb_6f levels in the mutant is therefore likely to cause HL sensitivity under photoautotrophic conditions. Moreover, while increasing the incident excitation energy had a marked impact on electron transport of the mutant (Figure 2a,b), it did not appear to further alter levels of Cytb_6f subunits (Figure 2c). We also observed reduced levels of Cytb_6f subunits in *cpld49* grown photoautotrophically in LL (Figure S4b), indicating that CPLD49 is required for Cytb_6f accumulation regardless of whether or not an external carbon source is present in the growth medium. To more firmly establish whether or not the phenotypes of CAL014.01.15 were caused by disruption of Cre16.g666050, encoding CPLD49 (e.g. no impact of disruption of neighboring genes), we examined two additional mutant lines containing insertions in Cre16.g666050 (*cpld49*-2 and *cpld49*-3). These mutants also exhibited reduced levels of Cytb_6f (Figure S5), confirming conclusions from the complementation results.

Loss of CPLD49 impairs electron transport, but does not markedly impact state transitions

Cytb_6f is a major hub for LEF and CEF, and forms a docking site for the STT7 kinase, which is associated with redox-dependent activation of state transitions (Gal *et al.*, 1987; Depège *et al.*, 2003). The state transition component of non-photochemical quenching helps balance light absorption between the photosystems and reduces redox pressure on electron transport (Wollman, 2001). Therefore, we probed whether diminished levels of Cytb_6f in *cpld49* during photoheterotrophic growth impacted the various activities associated with this complex. As a proxy for LEF (i.e. electron flow from water through PSII), we measured rates of light-dependent O_2 evolution, as well as rates of O_2 uptake in the dark, at different light intensities for HL-grown WT, *cpld49* and *cpld49-CPLD49* cells and determined levels of gross O_2 evolution. While all strains showed a light-dependent increase in gross O_2 evolution, the *cpld49* mutant had significantly lower rates than those

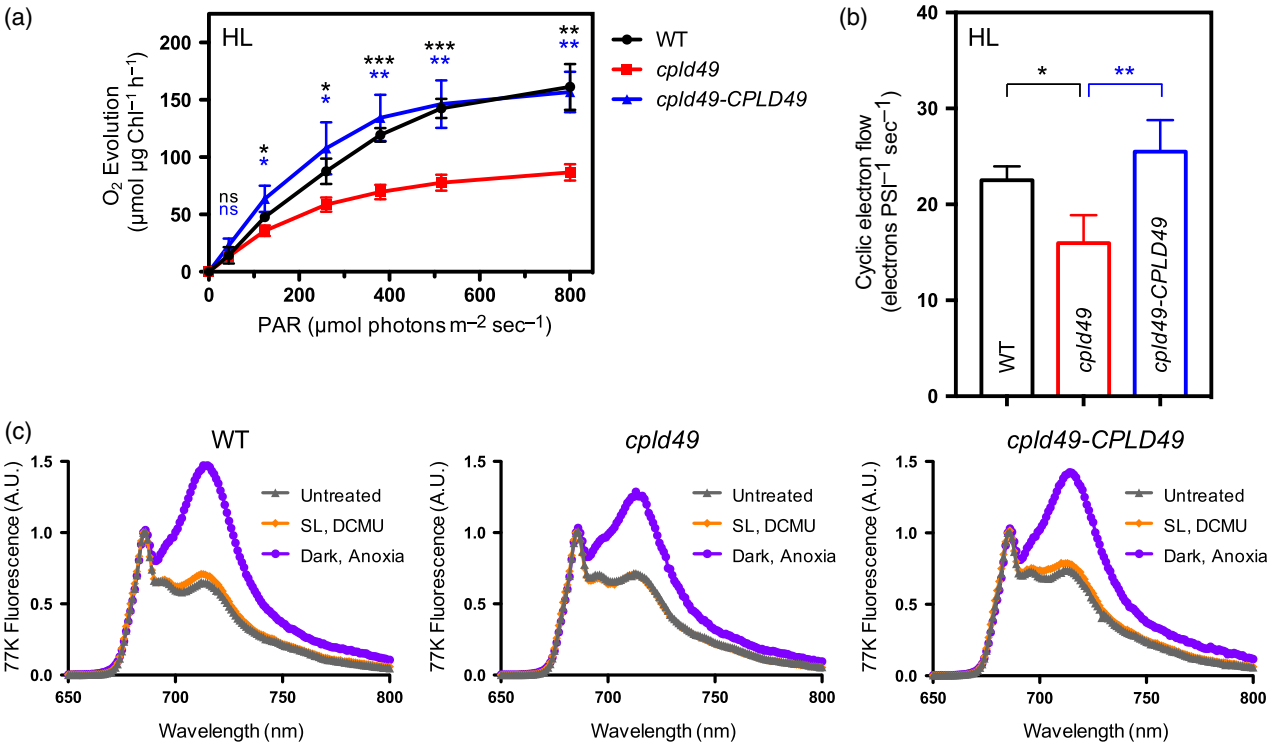

Figure 3. Loss of Cytb_6f restricts electron transport but does not compromise the ability of *cpld49* to perform state transitions.
(a) Measurements of gross photosynthetic O_2 evolution. Strains were grown photoheterotrophically in high light (HL), pelleted and then resuspended in photoautotrophic [Tris–Phosphate (TP)] medium; 2 mM $NaHCO_3$ was added to the cell suspension as an electron acceptor. The cells were maintained for 2 min at each light intensity, followed by a 2 min dark period, to generate the given rates. All O_2 evolution rates were corrected for respiratory O_2 uptake (see Experimental Procedures). PAR, photosynthetically active radiation. Average ± SD shown for three biological replicates. Statistical analysis was performed using Student's *t*-test. *P*-values indicate statistical significance between wild-type (WT) and *cpld49* (black asterisks) or *cpld49* and *CPLD49-CPLD49* (blue asterisks). ns, not significant; $*P \leq 0.05$; $**P \leq 0.01$; $***P \leq 0.001$.
(b) Measurements of cyclic electron flow (CEF). Strains were grown photoheterotrophically under HL, pelleted and resuspended in fresh Tris–Acetate–Phosphate (TAP) medium supplemented with 10% ficoll PM400. Measurements were performed on cultures exposed to 156 μmol photons m^{-2} sec^{-1} actinic light, as indicated in Experimental Procedures. CEF rates are an average of four biological replicates ± SD. Statistical analysis was performed using Student's *t*-test. *P*-values indicate statistical significance between the values of WT and *cpld49* (black asterisks) or *cpld49* and *CPLD49-CPLD49* (blue asterisks). Notations are as in (a).
(c) 77K fluorescence emission spectra. Strains were grown in TAP liquid medium in low light (LL) and collected during exponential growth phase. State 1 conditions: strong light (SL; 800 μmol photons m^{-2} sec^{-1}) in the presence of DCMU. State 2 conditions: dark, anoxia. A single biological replicate is shown, although essentially identical results were obtained for three biological replicates.

of WT and *cpld49-CPLD49* cells at light intensities above 100 μmol photons m^{-2} sec^{-1}, with an approximately two-fold decrease at light intensities above 300 μmol photons m^{-2} sec^{-1} (Figure 3a). These results suggest that when grown at light intensities below 100 μmol photons m^{-2} sec^{-1}, decreased accumulation of Cytb_6f in *cpld49* does not limit LEF. However, at higher photon flux densities the loss of CPLD49 impacts LEF. These results could explain the mutant's growth defect during photoautotrophic growth in HL (Figures 1c and S3). We also measured rates of CEF for WT, *cpld49* and *cpld49-CPLD49* following growth in HL conditions. The steady-state rate of CEF in *cpld49* was slightly decreased relative to that in WT and *cpld49-CPLD49* (*t*-test, $P < 0.05$), although this diminished activity was not as severe as the loss of LEF activity (Figure 3b). Lastly, because Cytb_6f serves as a docking site for the STT7 kinase, we assessed the ability of *cpld49* to undergo state transitions based on 77K fluorescence emission measurements. Similar to WT and *cpld49-CPLD49*, the mutant was in state 1 when the cells were maintained in LL or treated with DCMU in HL (a control condition that favors state 1; Figure 3c). Furthermore, when the cells were transferred to dark, anoxic conditions (control condition that induces state 2), all strains underwent a transition from state 1 to state 2 (Figure 3c). These results suggest that the reduced levels of Cytb_6f in *cpld49* restrict LEF, with some reduction in CEF, but do not alter the ability of the cells to undergo state transitions.

CPLD49 is dispensable for Cytb_6f transcript accumulation

To determine whether CPLD49 influences expression of chloroplast and nucleus genes encoding subunits of Cytb_6f, we measured levels of these transcripts in WT, *cpld49* and *cpld49-CPLD49* (Figure 4). Total RNA was isolated from cells grown photoheterotrophically in HL and the levels of specific transcripts quantified by reverse

transcriptase-quantitative polymerase chain reaction (RT-qPCR). Expression of three chloroplast genes (*PetA*, *PetB* and *PetD*) and two nucleus genes (*PETC* and *PETO*) encoding subunits of Cytb_6f was similar among the three strains (Figure 4). Hence, the reduced accumulation of Cytb_6f in *cpld49* is not the consequence of a transcriptional defect.

Cytb_6f remaining in *cpld49* is not degraded more rapidly than in WT

To determine whether the reduced level of Cytb_6f in *cpld49* was caused by accelerated protein degradation, we transferred LL, photoheterotrophically grown cells to HL for up to 24 h in the presence of chloramphenicol to inhibit chloroplast translation. Cells were collected at several time points following administration of the inhibitor, total cellular protein solubilized and resolved by SDS–PAGE, and the levels of PsbA (D1) and PetA (Cyt *f*) were immunologically examined. This analysis revealed a similar rate of PsbA turnover in WT, *cpld49* and *cpld49-CPLD49* (Figure 5a,b). Furthermore, the rate of Cyt *f* turnover did not appear to be strongly affected by the loss of CPLD49 (Figure 5a,b), although its initial level was lower in *cpld49* than in WT or *cpld49-CPLD49*. Therefore, the decreased accumulation of Cytb_6f in *cpld49* does not appear to be a consequence of accelerated protein degradation, but instead suggests a post-transcriptional defect in synthesis/assembly of the complex.

CPLD49 is associated with thylakoid membranes

CPLD49 has a predicted amino-terminal chloroplast transit peptide (amino acids 1–33; Figure 1; Tardiff *et al.*, 2012) and was experimentally demonstrated to be chloroplast-localized in Chlamydomonas (Terashima *et al.*, 2011). To validate the subcellular localization of CPLD49, we analyzed whole-cell lysates and purified thylakoid membranes from WT cells and found that CPLD49 was present in the thylakoid fraction, which was also highly enriched for integral thylakoid subunit PetA (Figure 6a). RbcL, a frequent contaminant of thylakoid membranes, was present at high levels in total protein lysates but not detected in thylakoid preparations (Figure 6a). In a similar experiment in which total membrane proteins were separated from soluble protein by centrifugation, we observed only a small amount of CPLD49 in the soluble fraction; the distribution of CPLD49 between the soluble and membrane fractions was similar to that of PetA (Figure 6b).

Salt washes of isolated thylakoid membranes were used to examine the association between CPLD49 and the membranes. Purified thylakoids were treated with solutions of salt having a range of chaotropic strengths (Figure 6c). Treatment with the weaker chaotropic salts (NaBr, NaCl and Na_2CO_3) did not extract CPLD49 from the membranes, while the stronger ones (NaSCN and NaOH) did (Figure 6c). This pattern was also observed for NDA2, a thylakoid membrane-associated NAD(P)H dehydrogenase involved in reduction of the PQ pool and in chlororespiration (Jans *et al.*, 2008; Desplats *et al.*, 2009; Saroussi *et al.*, 2016); like CPLD49, the NDA2 protein lacks predicted integral membrane domains. In contrast, the known integral membrane protein PsbA did not completely dissociate from the membranes even after treatment with the strong chaotropes (Figure 6c).

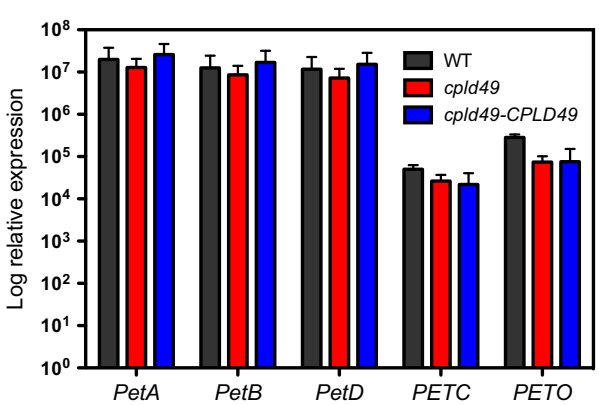

Figure 4. CPLD49 is dispensable for Cytb_6f transcript accumulation.
mRNA was collected from cells grown in high light (HL) for 24 h. Reverse transcriptase-quantitative polymerase chain reaction (RT-qPCR) analysis of specific Cytb_6f transcripts, including those from chloroplast (*PetA*, *PetB* and *PetD*) and nucleus (*PETC*, *PETO*) genes. Levels of individual transcripts were normalized to the housekeeping gene *CBLP*. Data represent average ± SD from three independent replicates.

CPLD49 co-migrates with CPLD38 on sucrose density gradients

We sought to determine whether CPLD49 interacts with specific thylakoid membrane protein complexes involved in photosynthesis. Thylakoid membranes isolated from WT cells grown photoheterotrophically in LL were solubilized with *n*-dodecyl-β-D-maltoside and solubilized complexes separated on a continuous sucrose gradient. Gradient fractions were collected and proteins in these fractions resolved by SDS–PAGE. Immunoblot analysis revealed that CPLD49 did not co-migrate with PSI, PSII or Cytb_6f (Figure 7a). Instead, it was present in a less dense fraction that contained free LHCs (released from PSI–LHCI or PSII–LHCII supercomplexes as a consequence of solubilization). CPLD49 was also present in the same fractions as CPLD38 (Figure 7a), another GreenCut protein implicated in Cytb_6f accumulation (Heinnickel *et al.*, 2013), raising the possibility that the two proteins are components of the same complex.

CPLD49 association with thylakoid membranes is eliminated in the *cpld38* mutant

To further explore the possibility that CPLD49 associates with CPLD38, we repeated thylakoid membrane fractionation experiments using the *cpld49* mutant and a mutant devoid of CPLD38 (*cpld38*; Heinnickel *et al.*, 2013). When

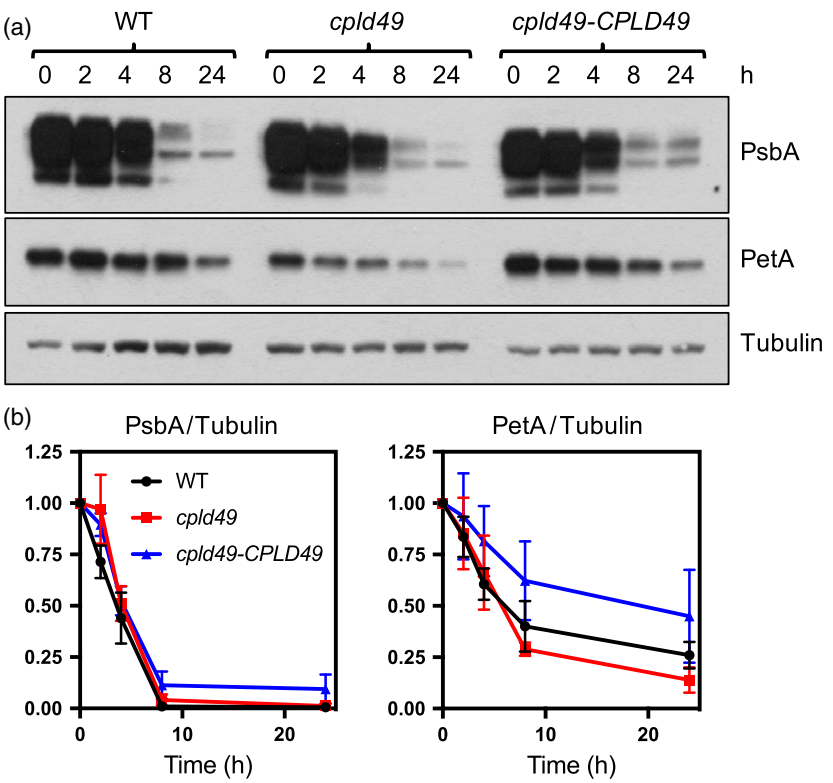

Figure 5. Loss of CPLD49 does not cause accelerated turnover of Cytb_6f subunits.
(a) Immunoblot assessment of the turnover of PSII and Cytb_6f subunits. Strains were grown photoheterotrophically in low light (LL), diluted to 5 μg Chl ml^{-1} in fresh Tris–Acetate–Phosphate (TAP) medium, and transferred to high light (HL); 100 μg ml^{-1} chloramphenicol was added to inhibit chloroplast translation. The characteristic turnover of the PsbA (D1) protein is shown as a positive control. PetA was used as the representative subunit of the Cytb_6f complex. Tubulin was used as a loading control.
(b) Time course of change of PsbA and PetA abundances (following addition of chloramphenicol) normalized to tubulin levels (loading control) at each time point. Data represent average ± SD from three independent replicates.

the same separations of solubilized thylakoid membranes from the *cpld38* mutant were examined, we no longer observed thylakoid association of CPLD49, even though it was still present in the total cell extract (Figure 7b). This raised the possibility that maintenance of CPLD49 on thylakoid membranes required association with CPLD38, a protein of the thylakoid membranes with two predicted transmembrane domains (TMDs; Heinnickel *et al.*, 2013), and can explain the finding that CPLD49 does not contain a predicted TMD and yet is not easily removed from the membranes (Figure 6c). To determine whether CPLD49 impacts thylakoid localization of CPLD38, we performed the reciprocal experiment with thylakoid membranes from the *cpld49* mutant and found that the absence of CPLD49 did not alter the thylakoid association of CPLD38 (Figure 7c). To further test a potential interaction between CPLD38 and CPLD49, we performed the yeast mating-based split ubiquitin assay with these proteins and found that they strongly interact (Figure 7d). Overall, these results indicate that CPLD38 and CPLD49 may be part of a novel thylakoid membrane protein complex that impacts accumulation of Cytb_6f and possibly affects other regulatory aspects of photosynthesis.

Targeted metabolomics suggest that CPLD49 is not a saccharopine dehydrogenase

Bioinformatic analyses raised the possibility that CPLD49 is a saccharopine dehydrogenase (Marchler-Bauer *et al.*, 2015), catalyzing the condensation of α-aminoadipate-δ-semialdehyde and glutamate to form saccharopine, which is then hydrolyzed to lysine and α-ketoglutarate (Broquist and Trupin, 1966). To explore whether CPLD49 has *in vivo* saccharopine dehydrogenase activity, we quantified metabolites that would be expected to accumulate in the absence of a functional saccharopine dehydrogenase (e.g. lysine, saccharopine, glutamate, α-aminoadipate), but did not observe any significant differences between WT and *cpld49*, except for some change in cysteine levels (Table S2). Therefore, CPLD49 does not likely function as a saccharopine dehydrogenase in Chlamydomonas, at least under our experimental conditions.

We detect no impact of CPLD49 loss on carotenoid accumulation

The Arabidopsis genome encodes three putative proteins with homology to saccharopine dehydrogenase and each has a distinct subcellular localization: AT4G33150 in the cytosol; AT5G39410 in mitochondria; and AT1G50450 in chloroplasts. While AT1G50450 encodes the protein most similar to Chlamydomonas CPLD49 (Tang *et al.*, 1997; Cunningham and Gantt, 2011), AT4G33150 is the only one of these related proteins for which saccharopine dehydrogenase activity was experimentally demonstrated (Tang *et al.*, 1997). Furthermore, Chlamydomonas CPLD49 and Arabidopsis AT1G50450 have homology to a dehydrogenase in *Adonis aestivalis* that is involved in converting β-

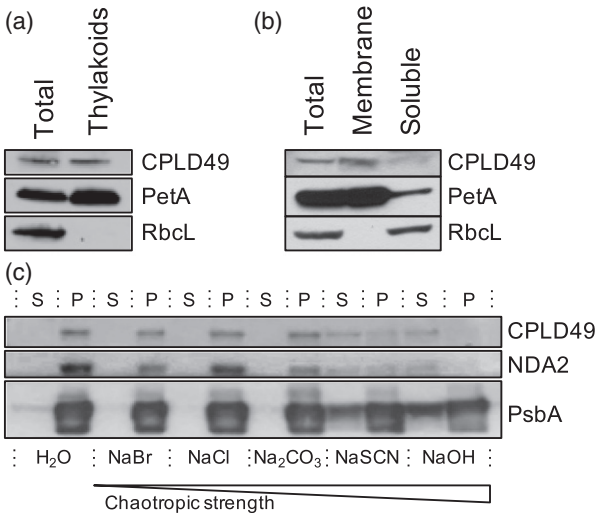

Figure 6. CPLD49 strongly associates with thylakoid membranes.
(a, b) Immunoblot analysis of total proteins (Total) and purified thylakoid membranes (Thylakoids) (a), and total protein, membrane protein and soluble proteins (b), all purified from low light (LL), photoheterotrophically grown wild-type (WT) cells. Equal Chl loaded in each lane.
(c) Immunological analysis of membrane versus soluble protein fractions from LL, photoheterotrophically grown WT cells after salt washes to assess the strength of the CPLD49 association with thylakoid membranes. Thylakoid membranes were purified from LL, photoheterotrophically grown WT cells and treated on ice for 30 min with H_2O (control), 1 M NaBr, 2 M NaCl, 0.1 M Na_2CO_3, 2 M NaSCN or 0.1 M NaOH. Dissociated proteins (S, supernatant) were separated from thylakoid membrane proteins (P, pellet) by low-speed centrifugation (1000 ***g***). Immunoblot analyses were performed for: CPLD49, 0 predicted transmembrane domains (TMDs); NDA2, thylakoid-associated protein involved in cyclic electron flow (CEF) and chlororespiration, 0 predicted TMDs; PsbA, D1 reaction center subunit of PSII, 5 TMDs.

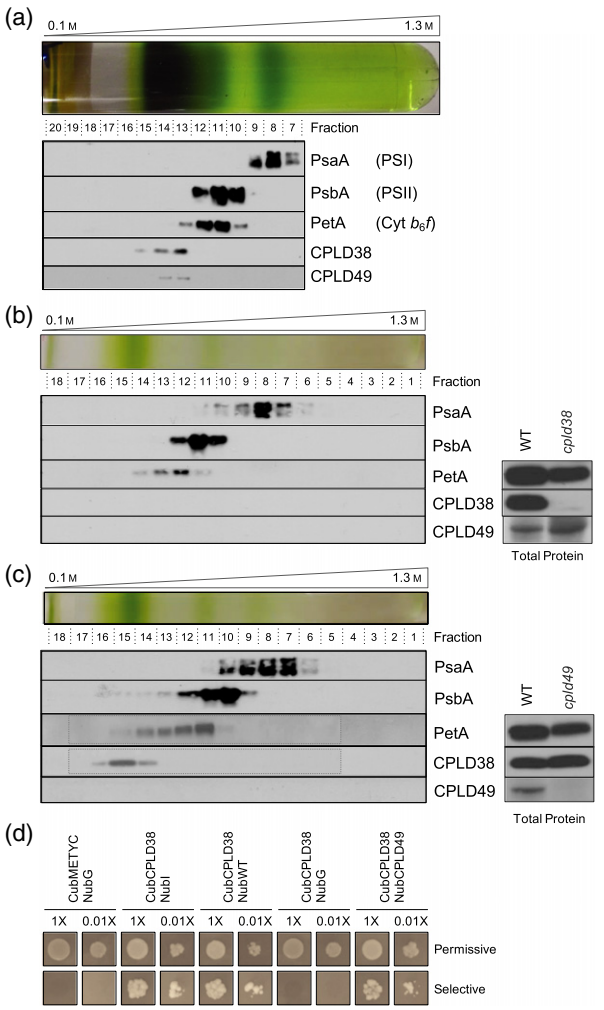

Figure 7. CPLD49 co-migrates with CPLD38, but not with PSI, PSII or Cytb_6f on sucrose gradients.
(a) Sucrose gradient fractionation of thylakoid membranes purified from wild-type (WT) cells grown photoheterotrophically in low light (LL). After β-DM treatment, solubilized thylakoids were overlaid on a 0.1–1.3 M continuous sucrose gradient and separated by ultracentrifugation. Fractions of equal volume were collected and analyzed by sodium dodecyl sulfate–polyacrylamide gel electrophoresis (SDS–PAGE) and immunoblotting.
(b) Sucrose gradient fractionation of thylakoid membranes from the *cpld38* mutant grown photoheterotrophically in LL. Total protein from WT and the *cpld38* mutant was also probed (right).
(c) Sucrose gradient fractionation of thylakoid membranes from *cpld49* grown photoheterotrophically in LL. Dashed boxes in PetA and CPLD38 immunoblots represent fractions 5–17 that were probed separately. Total protein from WT and the *cpld49* mutant was also examined (right).
(d) Interaction between CPLD49 and CPLD38 using the yeast mating-based split ubiquitin system (Grefen *et al.*, 2009). CubMETYC/NubG, negative control; CubCPLD38/NubI and CubCPLD38/NubWT, positive controls for strong interactions; CubCPLD38/NubG, control for weak interactions; CubCPLD38/NubCPLD49, for specific interactions. Permissive medium, diploid plates. Selective medium, MET0 plates.

carotene to the xanthophyll astaxanthin (Cunningham and Gantt, 2011). To explore whether CPLD49 is involved in the synthesis of a major or minor carotenoid, we made use of three highly sensitive high-performance liquid chromatography (HPLC) systems, each capable of detecting the presence of low-abundance pigments. All of the pigments that we detect in WT cells accumulated to similar levels in *cpld49* (Figure S6a–c). These results suggest that the defect in photosynthesis and Cytb_6f accumulation is not related to the absence of a specific carotenoid, although if it is an abundant carotenoid of which only one molecule localizes to the Cytb_6f complex in WT cells but not in the mutant, we would likely not be able to detect the change. We were also unable to detect a change in the pigment profile of the *cpld38* mutant relative to WT cells (Figure S6a–c).

DISCUSSION

The assembly and maintenance of photosynthetic pigment–protein complexes are highly regulated, and must be coordinated with cellular and environmental cues. Here, we describe the involvement of CPLD49, a highly conserved protein in the GreenCut, in the biogenesis of the photosynthetic apparatus. A strain devoid of CPLD49 is unable to grow without a fixed carbon source when exposed to HL. Moreover, CPLD49 associates with thylakoid membranes,

and has a critical role in maintaining photosynthetic activity and accumulation of the Cytb_6f complex.

A loss of nearly 90% of the Cytb_6f complex is evident in *cpld49* under both LL and HL (Figures 2c, S4 and S5). The complex remaining in the mutant transfers electrons (Figures 2a,b and 3a,b), supports state transitions (Figure 3c), and sustains photoautotrophic growth under LL and ML (Figures 1c and S3), suggesting that the complex that assembles in *cpld49* is functional. The observation that state transitions are not perturbed in *cpld49* is reasonable as previous work has shown an approximate stoichiometry of 1 STT7 kinase per 20 Cytb_6f complexes (Lemeille *et al.*, 2009). Growth of *cpld49* was not impaired when the cells were illuminated with LL or ML under photoheterotrophic and photoautotrophic growth conditions (Figures 1c and S3). Similarly, others have demonstrated that codon initiation mutants of the chloroplast *petD* gene accumulate 10–20% of Cytb_6f, but are still able to grow photoautotrophically in LL (Chen *et al.*, 1993). Moreover, LEF was not impaired when HL-grown *cpld49* was illuminated with LL (Figure 3a). However, when the growth light was increased above ~250 μmol photons m^{-2} sec^{-1}, the capacity to evolve O_2 in HL was almost twofold lower in *cpld49* than in WT and *cpld49-CPLD49* (Figure 3a), suggesting that the decreased levels of Cytb_6f in the mutant are insufficient to drive high rates of electron transfer. Interestingly, CEF rates under similar conditions were only 25–30% lower than those of the WT and *cpld49-CPLD49* (Figure 3b). Therefore, it appears that under elevated light conditions and in the presence of acetate, the Cytb_6f complex in the *cpld49* mutant can support CEF more efficiently than LEF, which may afford future opportunities to investigate electron partitioning between the two pathways.

Loss of the GreenCut protein CPLD38 in Chlamydomonas resulted in phenotypes similar to those of *cpld49*, including defects in accumulation of Cytb_6f and compromised photoautotrophic growth. However, unlike *cpld49*, the turnover rate of Cytb_6f subunits in *cpld38* appeared more rapid than in WT (Heinnickel *et al.*, 2013). A specific function for CPLD38 has not yet been determined. However, we demonstrate here that CPLD38 associates with thylakoid membranes and co-migrates with CPLD49 (but not with Cytb_6f) when purified thylakoid membranes are solubilized and the membrane complexes resolved by sucrose gradient centrifugation (Figure 7a). Furthermore, in the *cpld38* mutant, CPLD49 is not associated with thylakoids, suggesting that CPLD38 and CPLD49 may physically interact (Figure 7b). This possibility was supported by the finding that CPLD49 and CPLD38 positively interact in the yeast mating-based split ubiquitin assay (Figure 7d). Future biochemical/genetic and structural studies will help clarify specific aspects of these and other potential interactions. In Arabidopsis, the ortholog of CPLD38 (DAC) was also shown to be necessary for accumulation of Cytb_6f and to interact with subunit IV (chloroplast *petD* gene) of the complex (Xiao *et al.*, 2012). We did not find evidence suggesting that either CPLD38 or CPLD49 interacts with Cytb_6f in Chlamydomonas, though we cannot rule out the possibility that these proteins interact in a transient manner (e.g. during assembly of the complex) or that this interaction is disrupted by the procedures employed for purification and solubilization of thylakoid membranes.

Among green lineage organisms, the closest homologs of CPLD49 are annotated as saccharopine dehydrogenases. In plants and animals, saccharopine dehydrogenases catalyze the synthesis of saccharopine from α-ketoglutarate and L-lysine (Serrano *et al.*, 2012). This reaction may be critical for preventing accumulation of toxic levels of free lysine in plants (Arruda *et al.*, 2000). In contrast, fungi use saccharopine dehydrogenase to synthesize lysine (Serrano *et al.*, 2012). While Chlamydomonas may have multiple pathways for lysine synthesis (Vallon and Spalding, 2009), based on our metabolite analysis, we were unable to establish a role for CPLD49 in either lysine degradation or synthesis (Table S2).

CPLD49 is also related to an enzyme (carotenoid 4-hydroxy-β-ring 4-dehydrogenase, HBFD) involved in astaxanthin biosynthesis, a carotenoid found at high levels in the petals of some species of the genus Adonis (Cunningham and Gantt, 2011). HBFD in *A. aestivalis* is involved in the biosynthesis of astaxanthin from β-carotene (Cunningham and Gantt, 2011). Astaxanthin and other ketocarotenoids accumulate in Chlamydomonas zygospores where they may act as antioxidants (Lohr, 2009), but have not been identified in vegetative cells. Interestingly, Cytb_6f does bind pigments; each Cytb_6f monomer binds both a Chl *a* and a carotenoid molecule, probably β-carotene (Zhang *et al.*, 1999; Kurisu *et al.*, 2003; Stroebel *et al.*, 2003). Based on crystal structures, the carotenoid within the Cytb_6f complex is not close enough to the Chl to participate in triplet quenching and, thus, the roles of these pigments remain enigmatic (Dashdorj *et al.*, 2005). Furthermore, in certain cyanobacterial genomes the putative ortholog of *CPLD49* is contiguous to and probably in the same operon as a gene involved in carotenoid biosynthesis. This gene (*crtD*) encodes a carotenoid dehydrogenase related to the carotenoid isomerase CRTISO from green algae and land plants (Grossman *et al.*, 2004; Nisar *et al.*, 2015), that in tomato is involved in carotenoid isomerization through a reversible redox reaction (Isaacson *et al.*, 2002, 2004). These links between CPLD49 and carotenoid biosynthesis raise the possibility that CPLD49 is involved in modifying the carotenoid associated with Cytb_6f, which could account for reduced accumulation of this complex in the mutant. However, we did not observe differences in the abundances of either the major or minor pigments of *cpld49* relative to WT cells (Figure S6a–c), making it unclear whether or not CPLD49 functions in the

synthesis of a carotenoid. If it is involved in the synthesis of a minor carotenoid that co-migrates with other pigments, it may not be detected in the chromatographic and spectral analyses used. Furthermore, it is possible that CPLD49 is involved in the synthesis or modification of another class of chloroplast lipophilic compounds, such as the lipid/quinone constituents of thylakoids that associate with Cytb_6f. Alternatively, CPLD49 may have a role in the synthesis of cofactors needed for the biogenesis of Cytb_6f.

The assembly, structural stability and biological activity of membrane protein complexes depend on proper integration of lipids. Cytb_6f from Chlamydomonas has been successfully purified with its native lipids, revealing the presence of an associated acidic sulfoquinovosyldiacylglycerol (SQDG) molecule (Stroebel *et al.*, 2003). Interestingly, the sulfonate group of SQDG interacts with Lys^{272} of Cyt *f*, and Arg^{13} and Asn^{17} of the PETC Rieske iron-sulfur subunit (Stroebel *et al.*, 2003). Lys^{272} was previously shown to be a critical residue in controlling Cyt *f* synthesis, and its assembly and stability (Choquet *et al.*, 2003; de Vitry *et al.*, 2004). It was suggested that an extensive lipid-based network is required for the flexibility of the PETC subunit, which is critical for the transfer of electrons from the PQ pool to Cyt *f* (Hasan *et al.*, 2013; Hasan and Cramer, 2014). Cytb_6f in Chlamydomonas also contains two luminal-side lipids, potentially monogalactosyldiacylglycerol molecules (Stroebel *et al.*, 2003). Furthermore, computational modeling approaches have implicated other lipids, such as diacylglycerol in the structure of Cytb_6f (Hasan and Cramer, 2014). The 2.5 Å crystal structure of Cytb_6f from the cyanobacterium Nostoc PCC 7120 revealed the presence of at least 23 lipid-binding sites, which are thought to have a number of critical roles in electron transfer, complex and supercomplex formation, complex dimerization and facilitation of interactions with Chl *a* and carotenoid molecules (Hasan and Cramer, 2014). These results highlight a critical and as yet poorly understood role for lipids in the assembly and activity of Cytb_6f, and suggest that certain enzymatic reactions involving oxidation–reduction, such as that predicted for CPLD49, may be critical for creating the proper lipid context to sustain the activity and stability of macromolecular protein complexes integral to the membranes. On the other hand, short-chain dehydrogenases like CPLD49 may impact photosynthetic complexes indirectly through the control of various functions that occur in chloroplasts, such as translation initiation (Link *et al.*, 2012).

Conclusions

Overall, we have demonstrated a critical role for CPLD49, a conserved GreenCut protein, in photoautotrophic growth and accumulation of Cytb_6f. Recent studies on CPLD38 and its Arabidopsis homolog (Xiao *et al.*, 2012; Heinnickel *et al.*, 2013), together with our results, suggest that the GreenCut protein CPLD38 may act as a scaffold on thylakoid membranes that brings CPLD49 into close proximity to the Cytb_6f complex. Although still speculative, CPLD38 and CPLD49 may comprise a novel thylakoid complex involved in the synthesis/maturation of thylakoid lipophilic molecules and their incorporation into photosynthetic pigment–protein complexes. Additional information on the catalytic activity of these proteins is necessary to develop a better understanding of their precise roles in maintenance of photosynthetic function and Cytb_6f accumulation.

EXPERIMENTAL PROCEDURES

Chlamydomonas strains and culture conditions

A *C. reinhardtii* mutant with an insertion in the *CPLD49* gene (Cre16.g666050) was generated by random insertional mutagenesis of the WT 4A+ strain (CC-4051; Dent *et al.*, 2015). This mutant, CAL014.01.15 (*cpld49* throughout), was first identified in a forward genetic screen for strains affected in photosynthesis (Dent *et al.*, 2015). The insertion site in *cpld49* was confirmed by PCR using 5′ and 3′ border primers (Figure S1; Table S3). The *cpld49* mutant was backcrossed three times to 21gr mating type +/− (CC-1690 and CC-5119, respectively), and all experiments were conducted with 21gr+ as the WT genetic background. The ability of the mutant to grow using nitrate as a sole N source was confirmed after each backcross, which mitigated artifacts related to mutations in the *NIT2* locus (Wei *et al.*, 2014; Saroussi *et al.*, 2016). For complementation, the WT Cre16.g666050 (*CPLD49*) gene, including 1000 bp upstream (to obtain the native promoter) and 500 bp downstream (to obtain the native terminator), was amplified from WT genomic DNA. The PCR product was cloned into pSL18 (conferring resistance to paromomycin) and the linearized plasmid used to transform the *cpld49* mutant. Transformants were selected on TAP agar containing 6 μg ml^{-1} paromomycin (Figure S1c). The *cpld49* mutant (CC-5401), *cpld49-CPLD49* complemented strain (CC-5402) and the *cpld38* mutant (CC-5403) are available from the Chlamydomonas Resource Center (www.chlamy.org). Two additional mutants disrupted in Cre16.g666050 were isolated in a large-scale mutant library (https://www.chlamycollection.org/products/clip-strains/). These strains are referred to as *cpld49*-2 and *cpld49*-3, and are described in more detail in Figure S5.

Growth on solid and in liquid media

To assess growth on solid medium, strains were first grown in TAP (Harris, 1989) liquid medium to mid-late exponential phase (4–8 × 10^6 cells ml^{-1}) and subcultured for 24 h to maintain logarithmic growth. Cell densities were determined using a hemocytomer or a Beckman Coulter Counter (results were consistent between the two methods) and collected by centrifugation at 3220 ***g*** for 10 min at 20°C. Cell pellets were resuspended in TP liquid medium (same as TAP, but lacking acetate, buffered with HCl), 5 μl drops containing 1 × 10^5 cells were spotted onto either solid TP or TAP medium, and growth was assessed after 7 days. For growth in liquid medium, the strains were inoculated from plates, allowed to reach mid–late exponential phase and then subcultured for 24 h. Cells were centrifuged as above and resuspended in fresh TAP and TP medium to either a density of ~5 × 10^5 cells ml^{-1} or a Chl concentration of ~1 μg ml^{-1}. For growth curves, cells were counted using a Beckman Coulter Counter or a Countess automated cell counter (Invitrogen). Chl was

determined as previously described following extraction in 100% methanol (Porra *et al.*, 1989; Yang *et al.*, 2014).

Chlorophyll fluorescence

Cells were grown in TAP at 30 (LL) or 300 μmol photons m^{-2} sec^{-1} (HL) or in TP at LL for 24 h, collected by centrifugation (as above), resuspended in fresh medium to a concentration of 10 μg Chl ml^{-1} and dark-adapted with vigorous shaking for at least 20 min. Chl fluorescence transient induction kinetics were measured using a JTS10 spectrophotometer (Biologic); 1 mM $NaHCO_3$ was added as an electron acceptor. F_o, minimum fluorescence; F_m, maximum fluorescence in the dark-adapted state; F_m', maximum fluorescence at a given actinic light intensity; F′, fluorescence at a given actinic light intensity; F_v, variable fluorescence. The maximum quantum yield of PSII was measured in dark-adapted cultures grown in TAP, and is calculated as $F_v/F_m = (F_m - F_o)/F_m$. The quantum yield of PSII was measured at different actinic light intensities and is calculated as $\Phi PSII = (F_m' - F')/F_m'$.

Photosynthetic oxygen evolution

O_2 evolution and consumption were measured using a Clark-type electrode (Hansatech) at 20°C. Briefly, cells were grown photoheterotrophically in HL for 24 h and collected as described above. Prior to the measurements, cells were resuspended in photoautotrophic (TP) medium to a concentration of 10 μg Chl ml^{-1}. Cells (2 ml, totaling 20 μg Chl) were exposed to increasing light intensities (2 min for each intensity); each intensity was followed by a dark period. O_2 evolution and uptake were calculated using the slope values of the light and dark periods, respectively. Gross rates of photosynthetic O_2 evolution (shown as μmol O_2 mg Chl^{-1} h^{-1}) were obtained by subtracting the O_2 uptake rate in the dark (negative values) from the rate of O_2 evolution at the corresponding light intensity. Three biological replicates were used for each measurement.

Spectroscopic analysis and CEF

Absorbance changes associated with P_{700} oxidation–reduction were performed using a JTS10 spectrophotometer (Alric *et al.*, 2010; Wittkopp *et al.*, 2017). Cells were pelleted by centrifugation (1200 ***g***, 5 min, 20°C) and resuspended to a concentration of 25–30 μg ml^{-1} Chl in fresh medium supplemented with 10% ficoll PM400 (GE Healthcare). Dark-adapted cells were exposed to 156 μmol photons m^{-2} sec^{-1} during PSI oxidation followed by a saturating pulse, and a re-reduction period in the dark. Redox changes for P_{700} were monitored at 705 nm. Absorption changes measured at 740 nm were subtracted to correct for unspecific contributions to the 705 nm measurements; 10 μM DCMU and 1 mM hydroxylamine were added to the suspension to inhibit LEF prior to the measurement. The electrochromic shift following a laser flash or 4 ms continuous light (156 μmol photons m^{-2} sec^{-1}) was monitored using a 520 nm filter on the same samples as described above. CEF was calculated according to Takahashi *et al.* (2013). The ratio between PSI and PSII was estimated by measuring the 'a' phase of an electrochromic shift using a single turnover laser flash at 520 nm, both in the presence and absence of 10 μM DCMU and 1 mM hydroxylamine (Joliot and Delosme, 1974).

77K fluorescence

Aliquots of cells were collected and adjusted to 0.1 ± 0.01 absorbance at 440 nm by dilution in TAP medium before freezing in liquid N_2. Fluorescence emission was measured on frozen material using a Fluorolog-3 Fluorometer (Horiba Jobin-Yvon). Excitation of the sample was at 440 nm using a 4 nm excitation slit width; the emission was measured from 650 to 800 nm using a 2 nm emission slit width.

RNA extraction and quantification of Cytb_6f transcripts

Cells were grown in TAP for 24 h under HL, concentrated by centrifugation (3000 ***g***, 2 min, 4°C), and RNA was extracted from the cells (equivalent to 40 μg Chl) using Direct-zol RNA MiniPrep Plus kit (Zymo Research) according to the manufacturer's instructions. To analyze the relative abundance of *PetA*, *PetB*, *PetD*, *PETC* and *PETO* transcripts, 1 μg of RNA was reverse-transcribed using the iScript cDNA synthesis kit (BioRad). Gene-specific PCR primers with a Tm of ~60°C, GC content of ~50%, and PCR amplicon length that ranged from 125 to 200 bp were manually designed (Table S3). The efficiency of each primer pair was verified to be better than 98%. RT-qPCR was performed using a Lightcycler 480 (Roche). Reactions were performed in a final volume of 20 μl containing 10 μl SensiFast SYBR mix (Bioline), 4 nM of each primer and 0.05 μg of cDNA. PCR conditions were as follows: 3 min at 95°C followed by 40 cycles of 10 sec at 95°C and 30 sec at 60°C. Fluorescence threshold (Ct) was analyzed using Lightcycler 480 SW version 1.5 (Roche). Relative expression levels for all transcripts were compared with the *CBLP* housekeeping gene under the same conditions. The values reported for the expression data represent an average of three biological replicates ± SD according to Pfaffl (2001).

Protein isolation and immunoblot analysis

Total protein was extracted from cultures during mid-exponential growth phase by resuspending cells in 3 mM HEPES-KOH, pH 7.5, 60 mM dithiothreitol, 60 mM Na_2CO_3, 12% sucrose, 2% SDS, protease inhibitors, and boiling the sample for 50 sec. Samples were normalized to Chl content and proteins separated by SDS–PAGE on 10% polyacrylamide gels. Resolved proteins were transferred to PVDF membranes using a semidry blotting apparatus (Bio-Rad). For immunoblotting, membranes were blocked in TBS containing 0.1% Tween (TBST) and 5% milk for 1 h at 20°C. Primary antibodies were diluted in TBST 3% milk, and incubations of the membranes with the antibody solutions were performed overnight at 4°C. CPLD49 and CPLD38 antibodies were generated from oligopeptides CKTQPGVWYPEEKEALQDRRQ-amide and CDAD KQRKAAARAAAQQQQ-amide, respectively (Yenzym). All other antibodies were obtained from Agrisera, with the exception of Cyt *f* (from Francis-André Wollman) and NDA2 (from Xenie Johnson). Proteins were detected by enhanced chemiluminescence. Protein abundances were quantified using ImageJ (N.I.H.).

Isolation of thylakoid membranes

Cultures were grown as described above, and thylakoid membranes purified according to Takahashi *et al.* (2006). Briefly, 250 ml of cells in mid-exponential growth phase was pelleted by centrifugation (4225 ***g***, 10 min, 4°C), resuspended in Buffer 1 (25 mM HEPES-KOH, pH 7.5, 5 mM $MgCl_2$, 0.3 M sucrose, 0.2 mM PMSF, 1 mM benzamidine, 5 mM ε-amino-α-caproic acid) and broken using a French Pressure Cell at 500 PSI. Membranes were separated from the soluble phase of the cell by centrifugation at 2316 ***g*** (10 min, 4°C), and then resuspended and homogenized in Buffer 2 (5 mM HEPES-KOH, pH 7.5, 10 mM EDTA, 0.3 M sucrose, protease inhibitors as above) and centrifuged at 68 588 ***g*** (20 min, 4°C). The resulting pellet was resuspended in 5 ml Buffer 3 (5 mM HEPES-KOH, pH 7.5, 10 mM EDTA, 1.8 M sucrose, protease inhibitors as above), and overlaid with 2 ml Buffer 4 (same as solution

3, except 1.3 M sucrose) and then 5 ml Buffer 5 (5 mM HEPES-KOH, pH 7.5, 0.5 M sucrose). Thylakoid membranes were separated from unbroken cells, plasma membrane and chloroplast envelope by sucrose step-gradient ultracentrifugation (247 605 ***g***, 1 h, 4°C); the thylakoids were collected from the Buffer 3 (1.8 M sucrose)–Buffer 4 (1.3 M sucrose) interface, washed with 5 vol. of Buffer 6 (5 mM HEPES-KOH, pH 7.5, 10 mM EDTA, protease inhibitors as above) and collected by centrifugation (68 588 ***g***, 20 min, 4°C). The resulting thylakoid pellet was resuspended in 200 μl Buffer 6.

Separation of membrane and soluble proteins

Cells were grown and pelleted as above, resuspended in Buffer 1 (25 mM HEPES-KOH, pH 7.5, 5 mM $MgCl_2$, 0.3 M sucrose, 0.2 mM PMSF, 1 mM benzamidine, 5 mM ε-amino-α-caproic acid), and broken with a French Pressure Cell at 500 PSI. Membranes were separated from the soluble phase of the cell by centrifugation at 100 000 ***g*** for 1 h at 4°C. Soluble proteins were precipitated with saturated ammonium sulfate on ice for 30 min and collected by centrifugation at 2316 ***g*** for 10 min at 4°C. Membrane and soluble polypeptides were resolved by SDS–PAGE and specific polypeptides detected by immunoblotting, as described above.

Treatment of thylakoid membranes with chaotropic salt solutions

Thylakoid membranes were purified as described above and resuspended in Buffer 6 to a concentration of 0.655 mg Chl ml^{-1}. Thylakoids (10 μg Chl total) were incubated on ice in the dark for 30 min in the following solutions: water (control); 1 M NaBr; 2 M NaCl; 0.1 M Na_2CO_3; 2 M NaSCN; or 0.1 M NaOH. Soluble and membrane phases were separated by centrifugation (16 100 ***g***, 10 min, 4°C). The soluble phase (supernatant) was removed prior to detergent solubilization of the pelleted membrane proteins. Both soluble and membrane proteins were resolved by SDS–PAGE, and specific proteins detected by immunoblot analysis.

Sucrose gradient fractionation of thylakoid membrane protein complexes

Purified thylakoid membranes (0.8 mg Chl ml^{-1}) were solubilized with 0.75% (w/v) *n*-dodecyl-β-D-maltoside (β-DM) on ice in the dark for 40 min. Solubilized thylakoids were loaded onto a continuous sucrose density gradient (0.1–1.3 M sucrose, 5 mM Tricine-NaOH, pH 8, 0.05% β-DM) and the various pigment–protein complexes resolved by ultracentrifugation for 16 h at 288 000 ***g***, 4°C.

Yeast mating-based split ubiquitin system

CPLD49 and *CPLD38* genes (full-length, including chloroplast transit peptide sequences) were amplified from cDNAs and cloned in pENTR/D-TOPO (Invitrogen). The *CPLD49* gene from pENTR/D-TOPO_*CPLD49* was introduced into pNX22-DEST by LR cloning, while the *CPLD38* gene from pENTR/D-TOPO_*CPLD38* was introduced into pMetYC-DEST by LR cloning. An interaction between CPLD49 and CPLD38 was assessed by the yeast mating-based split ubiquitin system, as previously described (Yang *et al.*, 2015).

ACKNOWLEDGEMENTS

This work was supported by NSF Grant MCB 0951094, and the Office of Biological and Environmental Research, GTL Program, Office of Science, US Department of Energy Grants DE-FG02-07ER64427, DE-FG02-12ER16338 awarded to A.R.G. T.M.W. was supported in part by the National Institute of General Medical Sciences of the National Institutes of Health under award number T32GM007276. S.S. was supported by a Vaadia-BARD Postdoctoral Fellowship (United States-Israel Binational Agricultural Research and Development Fund, grant number FI-485-2013). Isolation and initial characterization of the *cpld49* mutant was supported by the US Department of Energy, Office of Science, Basic Energy Sciences, Chemical Sciences, Geosciences, and Biosciences Division under Field Work Proposal number 449B awarded to K.K.N. K.K.N. is an investigator of the Howard Hughes Medical Institute, and the Gordon and Betty Moore Foundation (through Grant GBMF3070).

CONFLICT OF INTEREST

The authors declare no conflict of interest.

AUTHOR CONTRIBUTIONS

T.M.W., S.S., X.J. and A.R.G. designed the experiments; T.M.W., S.S. and A.R.G. wrote the article with contributions of all the authors; T.M.W., S.S., W.Y., X.J., R.G.K., M.L.H., J.J.R., W.P., C.D.B., G.P. and M.L. performed experiments; T.M.W., S.S., W.Y., X.J., W.P., C.D.B., G.P., M.L. and A.R.G. analyzed data; R.M.D., K.K.N. and F.A.W. provided materials and/or technical assistance.

SUPPORTING INFORMATION

Additional Supporting Information may be found in the online version of this article.

Figure S1. Genotyping of the *cpld49* mutant and *cpld49-CPLD49* complemented strain.

Figure S2. The *cpld49* mutant is disrupted by a single pMS188 cassette.

Figure S3. Photoheterotrophic and photoautotrophic growth.

Figure S4. Chlorophyll fluorescence measurements and immunoblots for photoautotrophically grown cells.

Figure S5. Disruption of Cre16.g666050 in two independent strains results in reduced accumulation of Cyt*b6f*.

Figure S6. High-resolution HPLC analyses show no differences in abundances of either major or minor pigments between WT and *cpld49* or *cpld38* mutants.

Table S1. Predicted functions and localization of genes disrupted in the CAL014.01.15 strain (*cpld49* mutant).

Table S2. Targeted metabolomics analysis of *cpld49.*

Table S3. Primers used in this study.

REFERENCES

Alric, J., Lavergne, J. and Rappaport, F. (2010) Redox and ATP control of photosynthetic cyclic electron flow in *Chlamydomonas reinhardtii* (I) aerobic conditions. *Biochim. Biophys. Acta*, **1797**, 44–51.

Armbruster, U., Zühlke, J., Rengstl, B. *et al.* (2010) The Arabidopsis thylakoid protein PAM68 is required for efficient D1 biogenesis and photosystem II assembly. *Plant Cell*, **22**, 3439–3460.

Arruda, P., Kemper, E.L., Papes, F. and Leite, A. (2000) Regulation of lysine catabolism in higher plants. *Trends Plant Sci.* **5**, 324–330.

Baker, N.R. (2008) Chlorophyll fluorescence: a probe of photosynthesis in vivo. *Annu. Rev. Plant Biol.* **59**, 89–113.

Bhuiyan, N.H., Friso, G., Poliakov, A., Ponnala, L. and van Wijk, K.J. (2015) MET1 is a thylakoid-associated TPR protein involved in photosystem II supercomplex formation and repair in Arabidopsis. *Plant Cell*, **27**, 262–285.

Broquist, H.P. and Trupin, J.S. (1966) Amino acid metabolism. *Annu. Rev. Biochem.* **35**, 231–274.

Calderon, R.H., García-Cerdán, J.G., Malnoë, A., Cook, R., Russell, J.J., Gaw, C., Dent, R.M., de Vitry, C. and Niyogi, K.K. (2013) A conserved

rubredoxin is necessary for photosystem II accumulation in diverse oxygenic photoautotrophs. *J. Biol. Chem.* **288**, 26688–26696.

Chen, X., Kindle, K. and Stern, D. (1993) Initiation codon mutations in the Chlamydomonas chloroplast *petD* gene result in temperature sensitive photosynthetic growth. *EMBO J.* **12**, 3627–3635.

Chi, W., Ma, J. and Zhang, L. (2012) Regulatory factors for the assembly of thylakoid membrane protein complexes. *Philos. Trans. R Soc. B Biol. Sci.* **367**, 3420–3429.

Choquet, Y. and Vallon, O. (2000) Synthesis, assembly and degradation of thylakoid membrane proteins. *Biochimie*, **82**, 615–634.

Choquet, Y. and Wollman, F.A. (2002) Translational regulations as specific traits of chloroplast gene expression. *FEBS Lett.* **529**, 39–42.

Choquet, Y., Stern, D.B., Wostrikoff, K., Kuras, R., Girard-Bascou, J. and Wollman, F.A. (1998) Translation of cytochrome f is autoregulated through the 5′ untranslated region of petA mRNA in Chlamydomonas chloroplasts. *Proc. Natl Acad. Sci. USA*, **95**, 4380–4385.

Choquet, Y., Zito, F., Wostrikoff, K. and Wollman, F.A. (2003) Cytochrome *f* translation in Chlamydomonas chloroplast is autoregulated by its carboxy-terminal domain. *Plant Cell*, **15**, 1443–1454.

Cline, S.G., Laughbaum, I.A. and Hamel, P.P. (2017) CCS2, an octatricopeptide-repeat protein, is required for plastid cytochrome *c* assembly in the green alga *Chlamydomonas reinhardtii*. *Front. Plant Sci.* **8**, 1306. https://doi.org/10.3389/fpls.2017.01306.

Cunningham, F.X. and Gantt, E. (2011) Elucidation of the pathway to astaxanthin in the flowers of *Adonis aestivalis*. *Plant Cell*, **23**, 3055–3069.

Dashdorj, N., Zhang, H., Kim, H., Yan, J., Cramer, W.A. and Savikhin, S. (2005) The single chlorophyll *a* molecule in the cytochrome b_6f complex: unusual optical properties protect the complex against singlet oxygen. *Biophys. J.* **88**, 4178–4187.

Dent, R.M., Haglund, C.M., Chin, B.L., Kobayashi, M.C. and Niyogi, K.K. (2005) Functional genomics of eukaryotic photosynthesis using insertional mutagenesis of *Chlamydomonas reinhardtii*. *Plant Physiol.* **137**, 545–556.

Dent, R.M., Sharifi, M.N., Malnoë, A., Haglund, C., Calderon, R.H., Wakao, S. and Niyogi, K.K. (2015) Large-scale insertional mutagenesis of *Chlamydomonas* supports phylogenomic functional prediction of photosynthetic genes and analysis of classical acetate-requiring mutants. *Plant J.* **82**, 337–351.

Depège, N., Bellafiore, S. and Rochaix, J.D. (2003) Role of chloroplast protein kinase Stt7 in LHCII phosphorylation and state transition in Chlamydomonas. *Science*, **299**, 1572–1575.

Desplats, C., Mus, F., Cuinè, S., Billon, E., Cournac, L. and Peltier, G. (2009) Characterization of Nda2, a plastoquinone-reducing type II NAD(P)H dehydrogenase in *Chlamydomonas reinhardtii*. *J. Biol. Chem.* **284**, 4148–4157.

Dobáková, M., Sobotka, R., Tichý, M. and Komenda, J. (2009) Psb28 protein is involved in the biogenesis of the photosystem II inner antenna CP47 (PsbB) in the cyanobacterium *Synechocystis* sp. PCC 6803. *Plant Physiol.* **149**, 1076–1086.

Eberhard, S., Finazzi, G. and Wollman, F.A. (2008) The dynamics of photosynthesis. *Annu. Rev. Genet.* **42**, 463–515.

Fristedt, R., Williams-Carrier, R., Merchant, S.S. and Barkan, A. (2014) A thylakoid membrane protein harboring a DnaJ-type zinc finger domain is required for photosystem I accumulation in plants. *J. Biol. Chem.* **289**, 30657–30667.

Fristedt, R., Herdean, A., Blaby-Haas, C.E., Mamedov, F., Merchant, S.S., Last, R.L. and Lundin, B. (2015) PHOTOSYSTEM II PROTEIN33, a protein conserved in the plastid lineage, is associated with the chloroplast thylakoid membrane and provides stability to photosystem II supercomplexes in Arabidopsis. *Plant Physiol.* **167**, 481–492.

Gabilly, S.T., Dreyfuss, B.W., Karamoko, M., Corvest, V., Kropat, J., Page, M.D., Merchant, S.S. and Hamel, P.P. (2010) CCS5, a thioredoxin-like protein involved in the assembly of plastid *c*-type cytochromes. *J. Biol. Chem.* **285**, 29738–29749.

Gal, A., Shahak, Y., Schuster, G. and Ohad, I. (1987) Specific loss of LHCII phosphorylation in the Lemna mutant 1037 lacking the cytochrome b_6f complex. *FEBS Lett.* **221**, 205–210.

Gonzalez-Ballester, D., Pootakham, W., Mus, F. *et al.* (2011) Reverse genetics in Chlamydomonas: a platform for isolating insertional mutants. *Plant Methods*, **7**, 7–24.

Grefen, C., Obrdlik, P. and Harter, K. (2009) The determination of protein-protein interactions by the mating-based split-ubiquitin system (mbSUS). *Methods Mol. Biol.* **479**, 217–233.

Grossman, A.R., Lohr, M. and Im, C.S. (2004) *Chlamydomonas reinhardtii* in the landscape of pigments. *Annu. Rev. Genet.* **38**, 119–173.

Harris, E.H. (1989) *The Chlamydomonas Sourcebook. A Comprehensive Guide to Biology and Laboratory Use*. San Diego, CA: Academic Press.

Hartings, S., Paradies, S., Karnuth, B., Eisfeld, S., Mehsing, J., Wolff, C., Levey, T., Westhoff, P. and Meierhoff, K. (2017) The DnaJ-like zinc-finger protein HCF222 is required for thylakoid membrane biogenesis in plants. *Plant Physiol.* **174**, 1807–1824.

Hasan, S.S. and Cramer, W.A. (2014) Internal lipid architecture of the hetero-oligomeric cytochrome b_6f complex. *Structure*, **22**, 1008–1015.

Hasan, S.S., Yamashita, E. and Cramer, W.A. (2013) Transmembrane signaling and assembly of the cytochrome b_6f-lipidic charge transfer complex. *Biochem. Biophys. Acta*, **1827**, 1295–1308.

Heinnickel, M.L. and Grossman, A.R. (2013) The GreenCut: re-evaluation of physiological role of previously studied proteins and potentially novel protein functions. *Photosynth. Res.* **116**, 427–436.

Heinnickel, M.L., Alric, J., Wittkopp, T., Yang, W., Catalanotti, C., Dent, R., Niyogi, K.K., Wollman, F.A. and Grossman, A.R. (2013) Novel thylakoid membrane GreenCut protein CPLD38 impacts accumulation of the cytochrome b_6f complex and associated regulatory processes. *J. Biol. Chem.* **288**, 7024–7036.

Heinnickel, M., Kim, R.G., Wittkopp, T.M., Yang, W., Walters, K.A., Herbert, S.K. and Grossman, A.R. (2016) Tetratricopeptide repeat protein protects photosystem I from oxidative disruption during assembly. *Proc. Natl Acad. Sci. USA*, **113**, 2774–2779.

Inoue, K., Dreyfuss, B.W., Kindle, K.L., Stern, D.B., Merchant, S. and Sodeinde, O.A. (1997) *Ccs1*, a nuclear gene required for the post-translational assembly of chloroplast *c*-type cytochromes. *J. Biol. Chem.* **272**, 31747–31754.

Isaacson, T., Ronen, G., Zamir, D. and Hirschberg, J. (2002) Cloning of *tangerine* from tomato reveals a carotenoid isomerase essential for the production of beta-carotene and xanthophylls in plants. *Plant Cell*, **14**, 333–342.

Isaacson, T., Ohad, I., Beyer, P. and Hirschberg, J. (2004) Analysis in vitro of the enzyme CRTISO establishes a poly-cis-carotenoid biosynthetic pathway in plants. *Plant Physiol.* **136**, 4246–4255.

Jans, F., Mignolet, E., Houyoux, P.-A., Cardol, P., Ghysels, B., Cuiné, S., Cournac, L., Peltier, G., Remacle, C. and Franck, F. (2008) A type II NAD(P)H dehydrogenase mediates light-independent plastoquinone reduction in the chloroplast of Chlamydomonas. *Proc. Natl Acad. Sci. USA*, **105**, 20546–20551.

Joliot, P. and Delosme, R. (1974) Flash-induced 519 nm absorption change in green algae. *Biochim. Biophys. Acta*, **357**, 267–284.

Karamoko, M., Cline, S., Redding, K., Ruiz, N. and Hamel, P.P. (2011) Lumen Thiol Oxidoreductase1, a disulfide bond-forming catalyst, is required for the assembly of photosystem II in Arabidopsis. *Plant Cell*, **23**, 4462–4475.

Karpowicz, S.J., Prochnik, S.E., Grossman, A.R. and Merchant, S.S. (2011) The GreenCut2 resource, a phylogenomically derived inventory of proteins specific to the plant lineage. *J. Biol. Chem.* **286**, 21427–21439.

Kirst, H., García-Cerdán, J.G., Zurbriggen, A. and Melis, A. (2012) Assembly of the light-harvesting chlorophyll antenna in the green alga *Chlamydomonas reinhardtii* requires expression of the TLA2-CpFTSY gene. *Plant Physiol.* **158**, 930–945.

Kuras, R. and Wollman, F.A. (1994) The assembly of cytochrome b_6f complexes: an approach using genetic transformation of the green alga *Chlamydomonas reinhardtii*. *EMBO J.* **13**, 1019–1027.

Kuras, R., Saint-Marcoux, D., Wollman, F.A. and de Vitry, C. (2007) A specific *c*-type cytochrome maturation system is required for oxygenic photosynthesis. *Proc. Natl Acad. Sci. USA*, **104**, 9906–9910.

Kurisu, G., Zhang, H., Smith, J.L. and Cramer, W.A. (2003) Structure of the cytochrome b_6f complex of oxygenic photosynthesis: tuning the cavity. *Science*, **302**, 1009–1014.

Lemeille, S., Willig, A., Depège-Fargeix, N., Delessert, C., Bassi, R. and Rochaix, J.D. (2009) Analysis of the chloroplast protein kinase Stt7 during state transitions. *PLoS Biol.* **7**, e45. https://doi.org/10.1371/journal.pbio.1000045.

Link, S., Engelmann, K., Meierhoff, K. and Westhoff, P. (2012) The atypical short-chain dehydrogenases HCF173 and HCF244 are jointly involved in translational initiation of the psbA mRNA of Arabidopsis. *Plant Physiol.* **160**, 2202–2218.

Lohr, M. (2009) Carotenoids. In *The Chlamydomonas Sourcebook: Organellar and Metabolic Processes*, 2 edn, Vol. 2 (Stern, D.B. and Harris, E.H., eds). Dordrecht: Elsevier, pp. 799–817.

Lyska, D., Meierhoff, K. and Westhoff, P. (2013) How to build functional thylakoid membranes: from plastid transcription to protein complex assembly. *Planta*, **237**, 413–428.

Marchler-Bauer, A., Derbyshire, M.K., Gonzales, N.R. *et al.* (2015) CCD: NCBI's conserved domain database. *Nucleic Acids Res.* **43**, D222–D226.

Merchant, S.S., Prochnik, S.E., Vallon, O. *et al.* (2007) The Chlamydomonas genome reveals the evolution of key animal and plant functions. *Science*, **318**, 245–250.

Mininno, M., Brugière, S., Pautre, V., Gilgen, A., Ma, S., Ferro, M., Tardif, M., Alban, C. and Ravanel, S. (2012) Characterization of chloroplastic fructose 1,6-bisphosphate aldolases as lysine-methylated proteins in plants. *J. Biol. Chem.* **287**, 21034–21044.

Nickelsen, J. and Rengstl, B. (2013) Photosystem II assembly: from cyanobacteria to plants. *Annu. Rev. Plant Biol.* **64**, 609–635.

Nisar, N., Li, L., Lu, S., Khin, N.C. and Pogson, B.J. (2015) Carotenoid metabolism in plants. *Mol. Plant*, **8**, 68–82.

Pfaffl, M.W. (2001) A new mathematical model for relative quantification in real-time RT-PCR. *Nucleic Acids Res.* **29**, e45.

Pootakham, W., Gonzalez-Ballester, D. and Grossman, A.R. (2010) Identification and regulation of plasma membrane sulfate transporters in Chlamydomonas. *Plant Physiol.* **153**, 1653–1668.

Porra, R.J., Thompson, W.A. and Kriedemann, P.E. (1989) Determination of accurate extinction coefficients and simultaneous equations for assaying chlorophylls *a* and *b* extracted with four different solvents: verification of the concentration of chlorophyll standards by atomic absorption spectroscopy. *Biochim. Biophys. Acta*, **975**, 384–394.

Rochaix, J.D. (2004) Genetics of the biogenesis and dynamics of the photosynthetic machinery in eukaryotes. *Plant Cell*, **16**, 1650–1660.

Rochaix, J.D. (2011) Assembly of the photosynthetic apparatus. *Plant Physiol.* **155**, 1493–1500.

Saroussi, S.I., Wittkopp, T.M. and Grossman, A.R. (2016) The type II NADPH dehydrogenase facilitates cyclic electron flow, energy dependent quenching and chlororespiratory metabolism during acclimation of *Chlamydomonas reinhardtii* to nitrogen deprivation. *Plant Physiol.* **170**, 1975–1988.

Schöttler, M.A., Albus, C.A. and Bock, R. (2011) Photosystem I: its biogenesis and function in higher plants. *J. Plant Physiol.* **168**, 1452–1461.

Schult, K., Meierhoff, K., Paradies, S., Töller, T., Wolff, P. and Westhoff, P. (2007) The nuclear-encoded factor HCF173 is involved in the initiation of translation of the *psbA* mRNA in *Arabidopsis thaliana*. *Plant Cell*, **19**, 1329–1346.

Serrano, G.C., Rezende e Silva Figueira, T., Kiyota, E., Zanata, N. and Arruda, P. (2012) Lysine degradation through the saccharopine pathway in bacteria: LKR and SDH in bacteria and its relationship to the plant and animal enzymes. *FEBS Lett.* **586**, 905–911.

Stroebel, D., Choquet, Y., Popot, J.L. and Picot, D. (2003) An atypical haem in the cytochrome b_6f complex. *Nature*, **426**, 413–418.

Takahashi, H., Iwai, M., Takahashi, Y. and Minagawa, J. (2006) Identification of the mobile light-harvesting complex II polypeptides for state transitions in *Chlamydomonas reinhardtii*. *Proc. Natl Acad. Sci. USA*, **103**, 477–482.

Takahashi, H., Clowez, S., Wollman, F.A., Vallon, O. and Rappaport, F. (2013) Cyclic electron flow is redox-controlled but independent of state transition. *Nat. Commun.* **4**, 1954. https://doi.org/10.1038/ncomms2954.

Tang, G., Miron, D., Zhu-Shimoni, J.X. and Galili, G. (1997) Regulation of lysine catabolism through lysine-ketoglutarate reductase and saccharopine dehydrogenase in Arabidopsis. *Plant Cell*, **9**, 1305–1316.

Tardiff, M., Atteia, A., Specht, M. *et al.* (2012) PredAlgo: a new subcellular localization prediction tool dedicated to green algae. *Mol. Biol. Evol.* **29**, 3625–3639.

Terashima, M., Specht, M. and Hippler, M. (2011) The chloroplast proteome: a survey from the *Chlamydomonas reinhardtii* perspective with a focus on distinctive features. *Curr. Genet.* **57**, 151–168.

Vallon, O. and Spalding, M.H. (2009) Amino acid metabolism. In *The Chlamydomonas Sourcebook: Organellar and Metabolic Processes*, 2 edn, Vol. 2 (Stern, D.B. and Harris, E.H., eds). Dordrecht: Elsevier, pp. 115–158.

de Vitry, C., Ouyang, Y., Finazzi, G., Wollman, F.A. and Kallas, T. (2004) The chloroplast Rieske iron-sulfur protein: at the crossroads of electron transport and signal transduction. *J. Biol. Chem.* **279**, 44621–44627.

Wei, L., Derrien, B., Gautier, A. *et al.* (2014) Nitric oxide-triggered remodeling of chloroplast bioenergetics and thylakoid proteins upon nitrogen starvation in *Chlamydomonas reinhardtii*. *Plant Cell*, **26**, 353–372.

Wittenberg, G., Järvi, S., Hojka, M., Tóth, S.Z., Meyer, E.H., Aro, E.M., Schöttler, M.A. and Bock, R. (2017) Identification and characterization of a stable intermediate in photosystem I assembly in tobacco. *Plant J.* **90**, 478–490.

Wittkopp, T.M., Saroussi, S., Yang, W. and Grossman, A.R. (2016) The Greencut: functions and relationships of proteins conserved in green lineage organisms. In *Chloroplasts: Current Research and Future Trends* (Kirchhoff, H., ed). Norfolk: Caister Academic Press, pp. 239–276.

Wittkopp, T.M., Schmollinger, S., Saroussi, S. *et al.* (2017) Bilin-dependent photoacclimation in *Chlamydomonas reinhardtii*. *Plant Cell*, **29**, 2711–2726.

Wollman, F.A. (2001) State transitions reveal the dynamics and flexibility of the photosynthetic apparatus. *EMBO J.* **20**, 3623–3630.

Wollman, F.A., Minai, L. and Nechushtai, R. (1999) The biogenesis and assembly of photosynthetic proteins in thylakoid membranes. *Biochim. Biophys. Acta*, **1411**, 21–85.

Wostrikoff, K., Girard-Bascou, J., Wollman, F.A. and Choquet, Y. (2004) Biogenesis of PSI involves a cascade of translational autoregulation in the chloroplast of Chlamydomonas. *EMBO J.* **23**, 2696–2705.

Xiao, J., Li, J., Ouyang, M., Yun, T., He, B., Ji, D., Ma, J., Chi, W. and Zhang, L. (2012) DAC is involved in the accumulation of the cytochrome b_6f complex in Arabidopsis. *Plant Physiol.* **160**, 1911–1922.

Xie, Z., Culler, D., Dreyfuss, B.W., Kuras, R., Wollman, F.A., Girard-Bascou, J. and Merchant, S.S. (1998) Genetic analysis of chloroplast *c*-type cytochrome assembly in *Chlamydomonas reinhardtii*: one chloroplast locus and at least four nuclear loci are required for heme attachment. *Genetics*, **148**, 681–692.

Yang, W., Catalanotti, C., D'Adamo, S. *et al.* (2014) Alternative acetate production pathways in *Chlamydomonas reinhardtii* during dark anoxia and the dominant role of chloroplasts in fermentative acetate production. *Plant Cell*, **26**, 4499–4518.

Yang, W., Wittkopp, T.M., Li, X. *et al.* (2015) Critical role of *Chlamydomonas reinhardtii* Ferredoxin-5 in maintaining membrane structure and dark metabolism. *Proc. Natl Acad. Sci. USA*, **112**, 14978–14983.

Zhang, H., Huang, D. and Cramer, W.A. (1999) Stoichiometrically-bound β-carotene in the cytochrome b_6f complex of oxygenic photosynthesis protects against oxygen damage. *J. Biol. Chem.* **274**, 1581–1587.

